Investigation of electron irradiation-induced magnetism in layered MoS$_2$ single crystals

Sang Wook Han, Youngsin Park, Young Hun Hwang, Wang G. Lee, and S. C. Hong

---

Articles you may be interested in

Bias voltage-controlled ferromagnetism switching in undoped zinc oxide thin film memory device
Appl. Phys. Lett. **109**, 252103 (2016); 10.1063/1.4971308

Pressure and temperature-dependent Raman spectra of MoS2 film
Appl. Phys. Lett. **109**, 242101 (2016); 10.1063/1.4968534

Ultra-fine metal gate operated graphene optical intensity modulator
Appl. Phys. Lett. **109**, 251101 (2016); 10.1063/1.4972306

Route toward high-speed nano-magnonics provided by pure spin currents
Appl. Phys. Lett. **109**, 252401 (2016); 10.1063/1.4972244

Investigation of electron irradiation-induced magnetism in layered MoS$_2$ single crystals

Sang Wook Han,[1] Youngsin Park,[2] Young Hun Hwang,[3] Wang G. Lee,[2] and S. C. Hong[1,a)]

[1]*Department of Physics and Energy Harvest-Storage Research Center (EHSRC), University of Ulsan, Ulsan 44610, South Korea*
[2]*School of Natural Science, Ulsan National Institute of Science and Technology (UNIST), Ulsan 44919, South Korea*
[3]*School of Materials Science and Engineering, Ulsan National Institute of Science and Technology (UNIST), Ulsan 44919, South Korea*

By using higher acceleration energies than the displacement energy of Mo atoms, the electron irradiation on the layered MoS$_2$ single crystals is found to be an effective and simple method to induce the diamagnetic to ferromagnetic phase transition persisting up to room temperature. The easy axis can be controllable by regulating the electron dose and the acceleration energy. The ferromagnetic states are largely attributed to the strain around the vacancies. © 2016 Author(s). All article content, except where otherwise noted, is licensed under a Creative Commons Attribution (CC BY) license (http://creativecommons.org/licenses/by/4.0/). [http://dx.doi.org/10.1063/1.4971192]

Recently, the reduced dimensionality of transition metal dichalcogenides (TMDs) has gained renewed interest due to the successful realization of field-effect transistors[1] and the thickness-dependent, indirect-direct bandgap transition.[2,3] These findings have boosted the development of two-dimensional (2D) materials for high-performance flexible electronic and optoelectronic devices.[4,5] Additionally, the presence of defects in semiconducting MoS$_2$ has significantly affected the transport property.[6–9] Especially, defect engineering is essential to effectively manipulate magnetic property[10–14] in the diamagnetic 2H-MoS$_2$ for possible spintronics and quantum information devices.[15] However, although relatively large magnetic moments are realized at room temperature *via* a chemical method,[16,17] it is quite difficult to characterize the magnetic states of the monolayer or few-layer TMDs on the possible devices because of the strong diamagnetic substrates. More recently, electron irradiation with low energy (below 30 keV) has been used to improve both magnetic and electrical properties of MoS$_2$.[18] The approach using electron beam-based techniques enables the electronic structure to be engineered *via* tailoring the atomic structures.[19–22] Particularly, monosulfur vacancies (V$_S$'s) are frequently observed in transmission electron microscope (TEM) measurements,[23] where the electron beam (80 keV) is lower than the displacement energy of S atoms (90 keV) [Mo atoms (560 keV)]. A prolonged exposure, i.e., an increased electron dose, increases the vacancy concentration and evolves the V$_S$ defects into line defects.[24] On the basis of these results, the correlation between the electron irradiation-induced defects and the magnetic properties is crucial for the successful integration of MoS$_2$ into possible device. In this work, it is found that the electron irradiation on the layered MoS$_2$ single crystals is an effective and simple method to induce a large magnetic moments compared to the chemical methods.[25]

The natural-single crystalline MoS$_2$ samples (SPI) were snipped to the size of 3×4 mm^2 from a large piece. In order to take the clean surface, each sample was mechanically cleaved to have a thickness of approximately 100 μm and then the electron was irradiated on each sample in ambient conditions at room temperature. For comparison of the available acceleration energies, three electron irradiation facilities (ELV-8 and LINAC electron accelerators) were used with different exposure times. The area of the electron irradiation at the specific point of 400 ± 50 mm was of width 600 ± 20 × length 20 ± 5 mm^2 with beam diameter of 25–35 mm. The stability of the beam energy and dose was less than $\pm 5\%$. The electron dose was checked by the dosimeter films. The conditions of electron irradiation are summarized in Table I. The dc magnetic and hysteresis loop measurements were performed from 2 to 300 K using a SQUID magnetometer (MPMS XL-7). For the structural characterization, the pristine and electron beam-irradiated samples were measured by using TEM (JEM-2100F) with an energy of electron beam (200 keV).[26] The histogram of the atomic size distribution from the high-resolution TEM (HRTEM) images was estimated by employing the ImageJ program. The comparison of such statistical distribution between the pristine MoS$_2$ and electron-irradiated samples helps to elucidate the change of the atomic structure due to electron irradiation-induced

TABLE I. Conditions of electron irradiation. MoS$_2$ single crystals were irradiated by electron beams with different electron doses (kGy) at the two acceleration energies (E$_a$): a low energy [0.7 MeV, L(x)] and a high energy [2.0 MeV, H(x)]. N$_e$ indicates the number of electrons per unit area (cm^2).

Sample	Dose	N$_e$	E$_a$
L(i)	150	3.35×10^{14}	0.7
L(ii)	300	6.70×10^{14}	
L(iii)	600	1.39×10^{15}	
H(i)	100	1.58×10^{14}	2.0
H(ii)	250	3.94×10^{14}	

a)Author to whom correspondence should be addressed. Electronic mail: schong@ulsan.ac.kr

defects. The depth profiles of the time-of-flight secondary ion mass spectroscopy (ToF-SIMS) measurements (TOF SIMS 5) were obtained *via* Cs ion sputtering at 2 keV with a probing area of $200 \times 200 \, \mu m^2$.

Figure 1 shows the magnetization curves as a function of the magnetic field strength (H) up to ± 70 kOe at room temperature. Along the in-plane (the *ab*-plane) direction (Figs. 1(a) and 1(c)), the electron irradiation at a low acceleration energy reduces the negative slopes of the pristine MoS_2 with increasing the electron dose (Fig. 1(a)). The irradiation at high acceleration energies also further induces the diamagnetic to paramagnetic phase transition (Fig. 1(c)). This phase transition is quite similar with the 1 T-phase incorporated MoS_2 samples *via* the chemical method.[25] On the other hand, along the out-of-plane (perpendicular to the *ab*-plane) direction (Figs. 1(b) and 1(d)), the change in the magnetic properties along the out-of-plane direction is complicated. At low acceleration energies, the diamagnetic slopes of L(ii) and L(iii) are not reduced relative to that of L(i). Moreover, the electron irradiation at high acceleration energies causes enhanced diamagnetic susceptibility compared to pristine MoS_2 in proportion to the electron dose. It seems that, by increasing the electron dose and acceleration energy, magnetic anisotropy becomes apparent between the in-plane and out-of-plane directions. This contrasting change in the magnetic properties between both directions was also obtained at low temperature of 5 K (see supplementary material, Fig. S1) and in the temperature dependence (between 2 and 300 K) under the application of an external H of 10 kOe (Fig. S2, supplementary material). In connection with the TEM and ToF-SIMS results (Figs. 3 and 4), the electron beam-induced magnetic anisotropy implies

that the electron irradiation of the current condition affects a few surface layers of the cleaved MoS_2 single crystals.

For clarity, the linear slope of the diamagnetic or paramagnetic background was subtracted from the each magnetic susceptibility of Fig. 1 (Fig. S1, supplementary material). After adopting this method, a weak ferromagnetic state was obtained in the pristine MoS_2 (Fig. S3(a), supplementary material) due to the presence of the defects, as revealed in the previous study.[27] Figure 2 clearly shows ferromagnetic hysteresis loops except the case of the L(iii) sample, where the magnetic states of the in-plane and out-of-plane directions remain paramagnetic and relatively negligible, respectively. The less electron dose than that of L(iii) is recommended to achieve the ferromagnetic state. On the other hand, it is revealed that the H(ii) sample has the largest saturation magnetization at 5 K (Fig. 2(b)): 1.46 emu/g ($4.2 \times 10^{-2} \, \mu_B$/Mo) and 1.16 emu/g ($3.3 \times 10^{-2} \, \mu_B$/Mo) along the in-plane and out-of-plane directions, respectively. It is notable that the saturation magnetization has the relative error of $\pm 9\%$ from the procedure of the background subtraction. The coercivities of both directions are approximately 0.1 kOe (Fig. S4, supplementary material) When the temperature is increased from 5 to 300 K, the saturation magnetizations of both directions are decreased to 0.11 emu/g ($3.2 \times 10^{-3} \, \mu_B$/Mo) and 0.12 emu/g ($3.4 \times 10^{-3} \, \mu_B$/Mo), respectively. Furthermore, the change of the magnetizations along the out-of-plane direction depending on the electron dose and acceleration energy is supported by the atomic and magnetic force microscope (AFM and MFM) results taken at room temperature (Fig. S5, supplementary material).[14]

On the other hand, the easy axis is changed depending on the acceleration energy and the electron dose. At the low
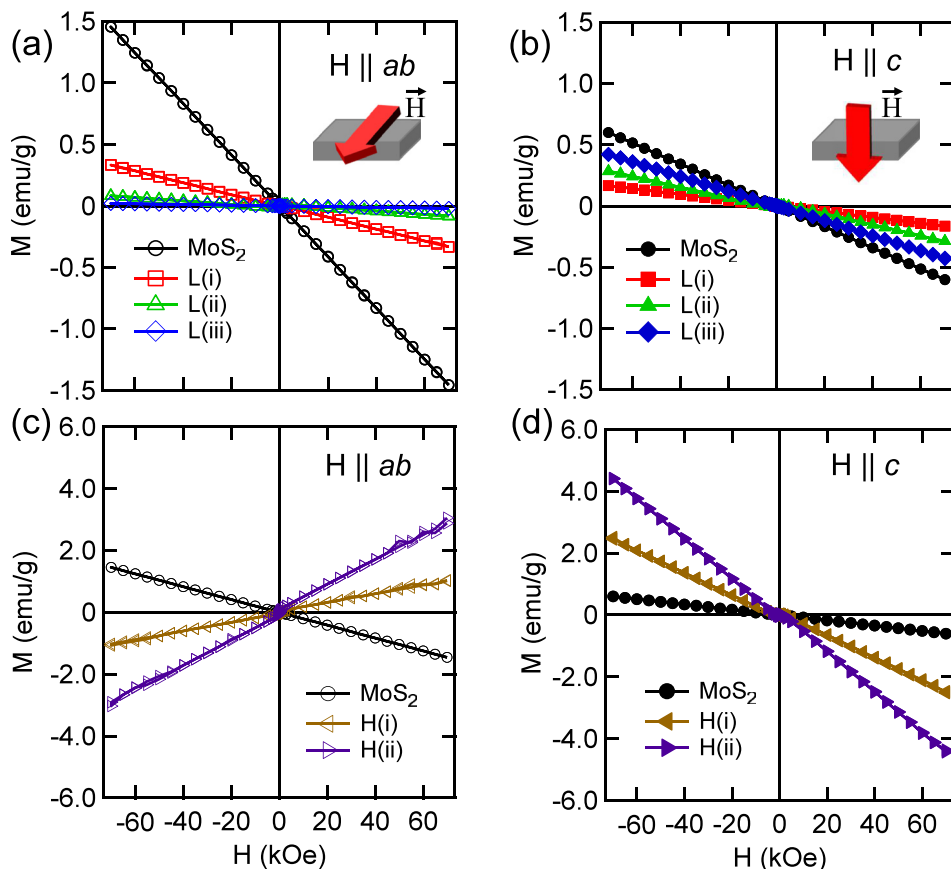

FIG. 1. Variation of the magnetization curves at 300 K for the pristine MoS_2 and electron beam-irradiated samples along the in-plane (a), (c) and out-of-plane (b), (d) directions, respectively.
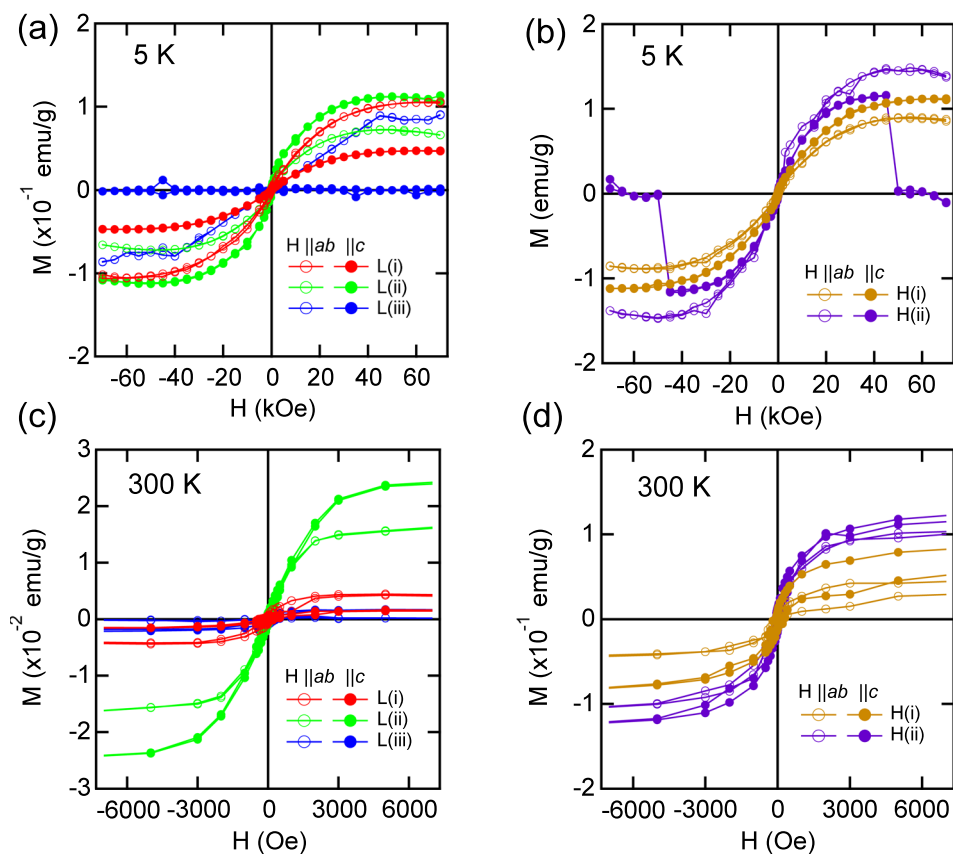
FIG. 2. Comparison of magnetization curves after subtracting the diamagnetic or paramagnetic background from the data of Figs. 1 and S1, supplementary material. The electron dose was changed at low (a), (c) and high (b), (d) acceleration energies (see Table I).
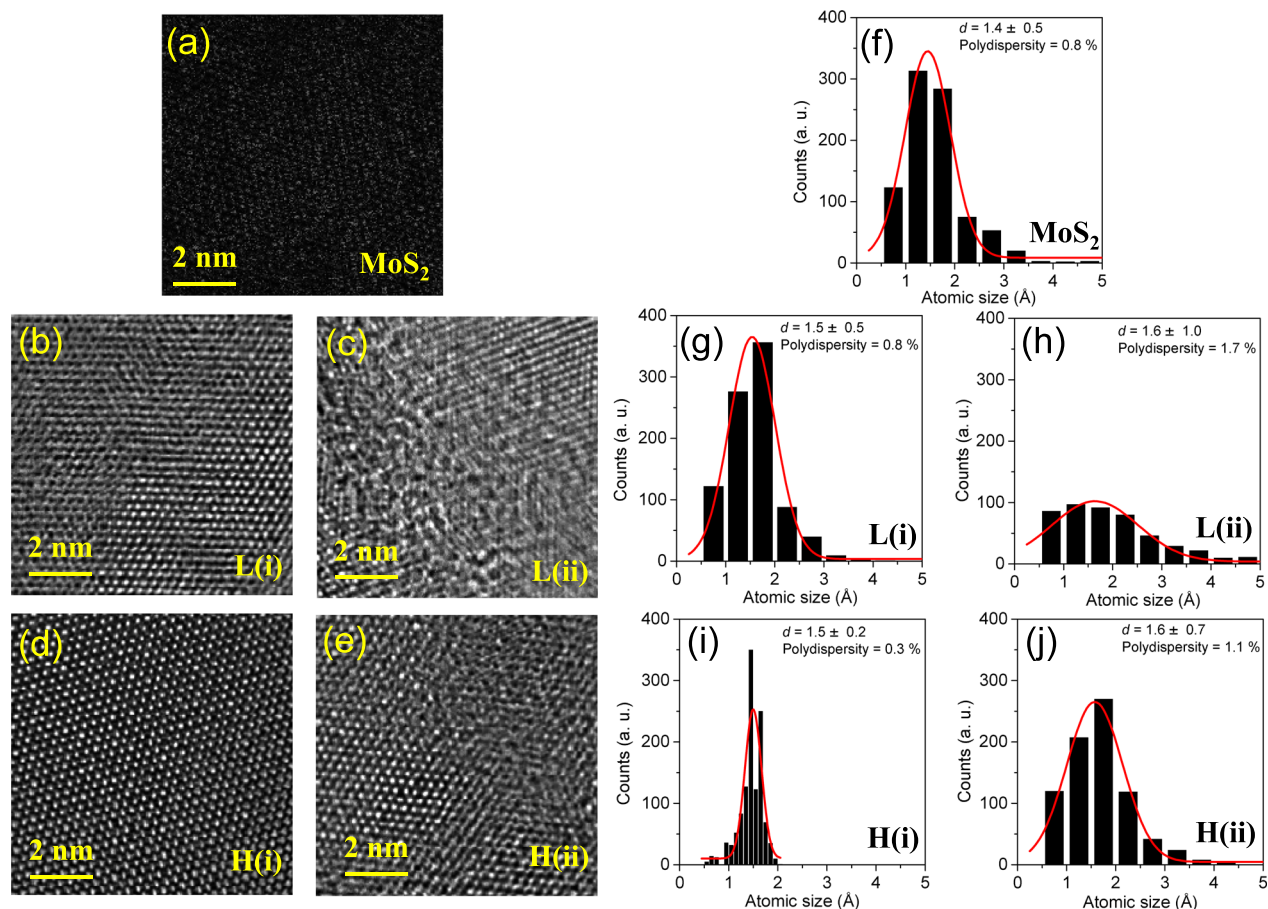

FIG. 3. HRTEM images of (a) the pristine MoS_2 and (b)–(e) electron beam-irradiated samples (see Figs. S4–S8, supplementary material). (f)–(j) Histograms summarize that the size distribution of the countable atoms after electron irradiation complies with a Gaussian profile (red curves) with the peak position centers at around 1.4 Å for the pristine MoS_2.

acceleration energy of 0.7 MeV (Figs. 2(a) and 2(c)), the easy axis of the L(i) and the L(ii) samples is obtained at the in-plane direction and the out-of-plane direction, respectively. At the high acceleration energy of 2.0 MeV (Figs. 2(b) and 2(d)), the easy axis of the H(i) sample is obtained at the out-of-plane direction. On the other hand, the easy axis of the H(ii) sample changes from the in-plane direction to the out-of-plane direction when the temperature increases from 5 to 300 K. The temperature-dependent easy axis of the H(ii) sample may be related to that of the abnormal diamagnetic states, which are retained at some condition of electron irradiation at much higher acceleration energy of 10 MeV (Figs. S3(b) and S3(c), supplementary material), varying the ferromagnetic Curie temperature between the in-plane and out-of-plane directions.

On the basis of our results, the coupling between the magnetic moments and controlled-defects below the acceleration energy of 30 keV (Ref. 18) seems to be relatively weak. In order to elucidate the correlation between the electron irradiation-induced defects and magnetic moments (or magnetic domains in Fig. S5, supplementary material), atomic structures on the electron-irradiated samples were investigated by using TEM. Figure 3 shows the HRTEM images of a pristine MoS_2 and electron beam-irradiated samples with the histogram of the atomic size distribution at each surface (see Figs. S6–S10, supplementary material for

details). The HRTEM image of the pristine MoS_2 (Fig. 3(a)) exhibits the V_S and line defects because the energy of electron beam of TEM is higher than the displacement energy of S atoms, as revealed in the previous studies.[23,24] There occasionally exist honeycomb lattices of 2H-MoS_2 (Fig. S6, supplementary material). The histogram of the L(i) sample (Fig. 3(g)) is quite similar to that of the pristine MoS_2 (Fig. 3(f)), together with the HRTEM images. This indicates that the influence of electron irradiation at this condition is comparable to the electron beam of TEM. In other words, the electron irradiation-induced defects are supposed to be hardly influenced by the TEM measurements.[26] On the other hand, the higher electron dose and acceleration energy than the electron beam energy of TEM (Figs. 3(b)–3(e)) increase various defects such as V_S and V_{S2} vacancies and Mo vacancies (V_{Mo}) (Figs. S7–S10, supplementary material). These defects are frequently obtained in the monolayer MoS_2 grown by an imperfect growth process.[28,29] Especially, the minimum polydispersity of the H(i) sample (Fig. 3(i)) indicates an average atomic diameter of 1.5 Å with a relatively narrow size distribution, and this condition is supposed to effectively create the V_{S2}-like defects (Fig. 3(d)). The ToF-SIMS results (Fig. 4) support that the higher acceleration energy effectively pushes away the S atoms, as compared with the low acceleration energy, even though the number of electrons in the dose of H(x) is less than half of that in of
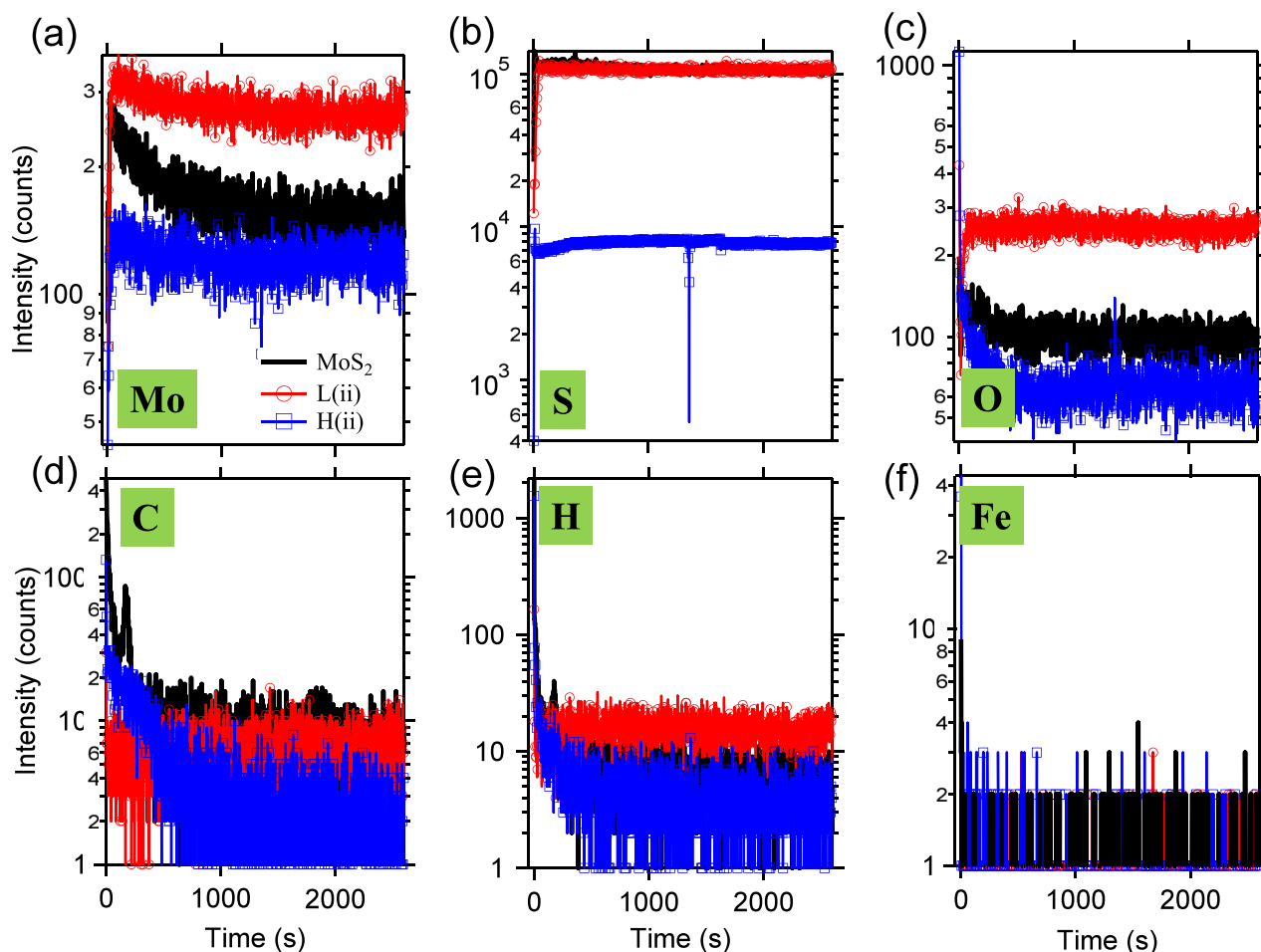

FIG. 4. ToF-SIMS depth profiles of the L(ii) and H(ii) samples were compared in the logarithmic scale with that of the pristine MoS_2; (a) molybdenum, (b) sulfur, (c) oxygen, (d) carbon, (e) hydrogen, and (f) iron.

L(x) (see Table I). Two samples (L(ii) and H(ii)) were investigated with the comparison of the pristine MoS_2. The possible (magnetic) impurities such as O, C, H, and Fe were found to mostly exist at the surfaces and possessed negligible intensities. The S counts in the H(ii) sample shows a reduced intensity compared with those of pristine MoS_2 and the L(ii) sample. On the other hand, the Mo count is slightly reduced, even at a much higher acceleration energy than the displacement energies of Mo atoms.[21,23]

Meanwhile, the theoretical study has reported that while the V_S, V_{S2}, and V_{MoS3} vacancies doped monolayer MoS_2 systems are nonmagnetic, the tensile strain induces magnetic moments in these systems by breaking of Mo-Mo metallic bonds around the vacancies.[30] In fact, the distances between the two neighboring Mo atoms around such vacancies increase in the electron irradiated samples compared to the distance $(a = 3.12 \text{ Å})$[26] of the pristine MoS_2 (Figs. S6–S10, supplementary material). The estimated tensile strains of the H(i) and H(ii) samples have increased to around 4.81% and 6.09%, respectively. Exceptionally, the compressive strain is obtained in the L(ii) sample (-5.77%). This contrasting strain effect is postulated to cause a considerable difference of the magnetizations between the L(x) and H(x) samples (Fig. 2). Additionally, the large magnetic moments and HRTEM image (Fig. S8, supplementary material) of the H(i) sample suggest that the non-magnetic V_{S2}-like defects[30] are much similar to the electron beam-induced 1 T phase[20] because the 1 T-phase incorporated MoS_2 samples *via* the chemical method induced the magnetism.[17,25] This may be a more simple way than a two-step hydrothermal method to intentionally introduce V_S defects, which transform the local lattice surrounding the V_S into 1 T phase.[17]

In summary, we have investigated the electron irradiation-induced magnetic phase transition and defects of the layered MoS_2 single crystals by changing the electron dose and the acceleration energy. The strain around vacancies is the crucial reason to have larger magnetic moments together with a possible 1 T phase incorporation at the certain condition of the H(i) sample. This simple electron irradiation provides a way to effectively manipulate magnetic property of the monolayer or few-layer TMDs for spintronics and quantum information devices.

See supplementary material for magnetic susceptibility at 5 K, temperature dependence of the magnetic susceptibility, magnetization curves of the pristine MoS_2 and electron irradiation at the acceleration energy of 10 MeV, AFM and MFM images, and characterization of the HRTEM.

[1]B. Radisavljevic, A. Radenovic, J. Brivio, V. Giacometti, and A. Kis, Nat. Nanotechnol. **6**, 147 (2011).

[2]A. Splendiani, L. Sun, Y. Zhang, T. Li, J. Kim, C.-Y. Chim, G. Galli, and F. Wang, Nano Lett. **10**, 1271 (2010).

[3]K. F. Mak, C. Lee, J. Hone, J. Shan, and T. F. Heinz, Phys. Rev. Lett. **105**, 136805 (2010).

[4]Q. H. Wang, K. Kalantar-Zadeh, A. Kis, J. N. Coleman, and M. S. Strano, Nat. Nanotechnol. **7**, 699 (2012).

[5]M. Xu, T. Liang, M. Shi, and H. Chen, Chem. Rev. **113**, 3766 (2013).

[6]A. M. van der Zande, P. Y. Huang, D. A. Chenet, T. C. Berkelbach, Y. M. You, G. H. Lee, T. F. Heinz, D. R. Reichman, D. A. Muller, and J. C. Hone, Nat. Mater. **12**, 554 (2013).

[7]H. Qiu, T. Xu, Z. Wang, W. Ren, H. Nan, Z. Ni, Q. Chen, S. Yuan, F. Miao, F. Song, G. Long, Y. Shi, L. Sun, J. Wang, and X. Wang, Nat. Commun. **4**, 2642 (2013).

[8]M. Ghorbani-Asl, A. N. Enyashin, A. Kuc, G. Seifert, and T. Heine, Phys. Rev. B **88**, 245440 (2013).

[9]S. McDonnell, R. Addou, C. Buie, R. M. Wallace, and C. L. Hinkle, ACS Nano **8**, 2880 (2014).

[10]J. Zhang, J. M. Soon, K. P. Loh, J. Yin, J. Ding, M. B. Sullivian, and P. Wu, Nano Lett. **7**, 2370 (2007).

[11]Y. Li, Z. Zhou, S. Zhang, and Z. J. Chen, J. Am. Chem. Soc. **130**, 16739 (2008).

[12]R. Shidpour and M. Manteghian, Nanoscale **2**, 1429 (2010).

[13]S. Mathew, K. Gopinadhan, T. K. Chan, X. J. Yu, D. Zhan, L. Gao, A. Rusydi, M. B. H. Breese, S. Dhar, Z. X. Shen, T. Venkatesan, and T. L. John, Appl. Phys. Lett. **101**, 102103 (2012).

[14]S. W. Han, Y. H. Hwang, S.-H. Kim, W. S. Yun, J. D. Lee, M. G. Park, S. Ryu, J. S. Park, D.-H. Yoo, S.-P. Yoon, S. C. Hong, K. S. Kim, and Y. S. Park, Phys. Rev. Lett. **110**, 247201 (2013).

[15]J.-R. Chen, P. M. Odenthal, A. G. Swartz, G. C. Floyd, H. Wen, K. Y. Luo, and R. K. Kawakami, Nano Lett. **13**, 3106 (2013).

[16]Z. Yang, D. Gao, J. Zhang, Q. Xu, S. Shi, K. Tao, and D. Xue, Nanoscale **7**, 650 (2015).

[17]L. Cai, J. He, Q. Liu, T. Yao, L. Chen, W. Yan, F. Hu, Y. Jiang, Y. Zhao, T. Hu, Z. Sun, and S. Wei, J. Am. Chem. Soc. **137**, 2622 (2015).

[18]D. Karmakar, R. Halder, N. Padma, G. Abraham, K. Vaibhav, M. Ghosh, M. Kaur, D. Bhattacharya, and T. V. Chandrasekhar Rao, J. Appl. Phys. **117**, 135701 (2015).

[19]M. José-Yacamán, H. López, P. Santiago, D. H. Galván, I. L. Garzón, and A. Reyes, Appl. Phys. Lett. **69**, 1065 (1996).

[20]Y.-C. Lin, D. O. Dumcenco, Y.-S. Huang, and K. Suenaga, Nat. Nanotechnol. **9**, 391 (2014).

[21]X. Liu, T. Xu, X. Wu, Z. Zhang, J. Yu, H. Qiu, J.-H. Hong, C.-H. Jin, J.-X. Li, X.-R. Wang, L.-T. Sun, and W. Guo, Nat. Commun. **4**, 1776 (2013).

[22]J. Lin, O. Cretu, W. Zhou, K. Suenaga, D. Prasai, K. I. Bolotin, N. T. Cuong, M. Otani, S. Okada, A. R. Lupini *et al.*, Nat. Nanotechnol. **9**, 436 (2014).

[23]H.-P. Komsa, J. Kotakoski, S. Kurasch, O. Lehtinen, U. Kaiser, and A. V. Krasheninnikov, Phys. Rev. Lett. **109**, 035503 (2012).

[24]H.-P. Komsa, S. Kurasch, O. Lehtinen, U. Kaiser, and A. V. Krasheninnikov, Phys. Rev. B **88**, 035301 (2013).

[25]S. Yan, W. Qiao, X. He, X. Guo, L. Xi, and W. Zhong, Appl. Phys. Lett. **106**, 012408 (2015).

[26]S. W. Han, W. S. Yun, J. D. Lee, Y. H. Hwang, J. Baik, H. J. Shin, W. G. Lee, Y. S. Park, and K. S. Kim, Phys. Rev. B **92**, 241303(R) (2015).

[27]S. Tongay, S. S. Varnoosfaderani, B. R. Appleton, J. Wu, and A. F. Hebard, Appl. Phys. Lett. **101**, 123105 (2012).

[28]W. Zhou, X. Zou, S. Najmaei, Z. Liu, Y. Shi, J. Kong, J. Lou, P. M. Ajayan, B. I. Yakobson, and J.-C. Idrobo, Nano Lett. **13**, 2615 (2013).

[29]J. Hong, Z. Hu, M. Probert, K. Li, D. Lv, X. Yang, L. Gu, N. Mao, Q. Feng, L. Xie, J. Zhang, D. Wu, and Z. Zhang, Nat. Commun. **6**, 6293 (2015).

[30]H. Zheng, B. Yang, D. Wang, R. Han, X. Du, and Y. Yan, Appl. Phys. Lett. **104**, 132403 (2014).